

Alma Mater Studiorum Università di Bologna
Archivio istituzionale della ricerca

Rotational spectroscopy of rare iron monoxide isotopologues: A mass-independent analysis

This is the final peer-reviewed author's accepted manuscript (postprint) of the following publication:

Published Version:

Björn Waßmuth, Alexander A. Breier, Mattia Melosso, Guido W. Fuchs, Thomas F. Giesen (2020). Rotational spectroscopy of rare iron monoxide isotopologues: A mass-independent analysis. MOLECULAR PHYSICS, 118(19-20), 1-9 [10.1080/00268976.2020.1774087].

Availability:

This version is available at: <https://hdl.handle.net/11585/900739> since: 2022-11-08

Published:

DOI: <http://doi.org/10.1080/00268976.2020.1774087>

Terms of use:

Some rights reserved. The terms and conditions for the reuse of this version of the manuscript are specified in the publishing policy. For all terms of use and more information see the publisher's website.

This item was downloaded from IRIS Università di Bologna (<https://cris.unibo.it/>).
When citing, please refer to the published version.

(Article begins on next page)

This is the final peer-reviewed accepted manuscript of:

Björn Waßmuth , Alexander A. Breier , Mattia Melosso , Guido W. Fuchs, and Thomas F. Giesen (2020). "Rotational spectroscopy of rare iron monoxide isotopologues: A mass-independent analysis", *Molecular Physics*.

The final published version is available online at:
<https://doi.org/10.1080/00268976.2020.1774087>

Terms of use:

Some rights reserved. The terms and conditions for the reuse of this version of the manuscript are specified in the publishing policy. For all terms of use and more information see the publisher's website.

This item was downloaded from IRIS Università di Bologna (<https://cris.unibo.it/>)

When citing, please refer to the published version.

Rotational spectroscopy of rare iron monoxide isotopologues: A mass-independent analysis

Björn Waßmuth^a, Alexander A. Breier^a, Mattia Melosso^b, Guido W. Fuchs^a and Thomas F. Giesen^a

^aLaboratory for Astrophysics, Institute of Physics, University of Kassel, Heinrich-Plett-Straße 40, D-34132 Kassel, Germany;

^bDipartimento di Chimica 'Giacomo Ciamician', Università di Bologna, via F. Selmi 2, I-40126 Bologna, Italy

ARTICLE HISTORY

Compiled May 14, 2020

Dedicated to Jürgen Gauss on the occasion of his 60th birthday.

ABSTRACT

We present pure rotational transitions of the rare iron monoxide isotopologues¹ ⁵⁷FeO, ⁵⁸FeO, and ⁵⁶Fe¹⁸O in their lowest spin states ⁵Δ₄. For ⁵⁷FeO the rotational spectrum reveals hyperfine splitting due to the nuclear spin of $I(^{57}\text{Fe}) = 1/2$. We use Dunham-like parameters to analyse the new laboratory data together with data from the literature. In particular, we are able to derive the Born-Oppenheimer breakdown parameters $\Delta_{U01}^{\text{Fe}} = -9.886(24)$ and $\Delta_{U01}^{\text{O}} = -10.761(67)$ and the corresponding equilibrium bond length of $r_e^{\text{BO}} = 1.6160302(20) \cdot 10^{-10}$ m. With these new accurate molecular parameters line positions on a sub-MHz accuracy level can be calculated, including those of the radioactive isotopologue ⁶⁰FeO. The new data allows for an astronomical search for the rare FeO isotopologues using sensitive radio telescopes, like the Atacama Large Millimeter/submillimeter Array (ALMA).

KEYWORDS

FeO; mm-wave; Radioactive Molecule; Supersonic jet expansion; Dunham.

1. Introduction

As early as 1945 the iron monoxide main isotopologue, ⁵⁶FeO, has been studied in the visible spectral region [1]. First rotationally resolved spectra of the 'orange bands' around 530 – 660 nm were published by Dhumwad *et al.* [2] in 1966. At that time, the electronic ground state of the molecule was not known. Barrow and Senior [3] proposed ⁵Σ or ⁷Σ as the most likely electronic ground state. Based on *ab initio* calculations Bagus and Preston [4] concluded that ⁵Σ⁺ cannot be the electronic ground state. Further experimental studies authored by West [5], Engelking [6], and Green [7] and finally laser induced fluorescence (LIF) measurements by Cheung *et al.* [8] showed that the electronic ground state of FeO is X⁵Δ_i. The rotational spectrum of an open

CONTACT Björn Waßmuth Email: b.wassmuth@physik.uni-kassel.de

¹In this article O is used for the oxygen main isotope ¹⁶O. All other oxygen isotopes are labelled explicitly.

shell radical in its $X^5\Delta_i$ ground state is complicate. Most of the diatomic iron bearing molecules have a high spin multiplicity in their electronic ground states due to the complexity of the d -electron shell of the iron atom. In the case of iron monoxide, the various low lying electronic states have been the subject of many studies in the visible region [9–16], and the near infrared region [17] as well as of theoretical calculations [18–22].

First pure rotational spectra in the mm-wave region were recorded by Endo *et al.* [23]. Their observations revealed transitions of the three lowest spin states ($^5\Delta_4$, $^5\Delta_3$, and $^5\Delta_2$). Kröckertskothén *et al.* [24] extended these data using microwave optical double resonance spectroscopy. Taylor *et al.* [17] measured the ground state Λ -doubling in the $\Omega = 1$ and $\Omega = 0$ components by means of Fourier transform spectroscopy. Pure rotational data of all five spin states of the main isotopologue, ^{56}FeO , including Λ doubling, and transitions in some spin states of ^{54}FeO have been measured by Allen *et al.* [25]. From optical Stark spectroscopy the permanent electric dipole moments $\mu(X^5\Delta_4) = 4.50 \pm 0.03$ D and $\mu(X^5\Delta_3) = 4.29 \pm 0.05$ D were derived [26].

Beside the main isotope ^{56}Fe , which makes 91.75 % of the natural abundance of iron on earth, three less abundant stable iron isotopes, namely ^{54}Fe (5.85 %), and the 'rare' isotopes ^{57}Fe (2.12 %), and ^{58}Fe (0.28 %) exist [28]. In contrast to the main isotopologue, ^{56}FeO , there is little information of other isotopologues. Spectroscopic data for ^{54}FeO and ^{57}FeO in the visible spectrum were measured by Barnes *et al.* [13]. Due to the lack of isotopic data, a previous attempt failed, to describe iron monoxide mass independently [25]. Here, we report on a dedicated laboratory study on some rare FeO isotopologues, which for the first time allows the mass independent description of FeO based on a Dunham-like approach which has been described in detail in [29–31]. The accuracy of the proposed method depends on the availability of spectra from different isotopologues. We present first pure rotational transitions of ^{57}FeO , ^{58}FeO , and $^{56}\text{Fe}^{18}\text{O}$ in the lowest spin state $^5\Delta_4$. The rotational spectrum of ^{57}FeO shows a hyperfine splitting due to the nuclear spin of iron $I(^{57}\text{Fe}) = 1/2$.

Iron is also an important element in space. From the relatively high cosmic abundances of the elements iron and oxygen [32–34] one would expect to readily detect small iron bearing molecules in the spectra of the circumstellar envelopes of red giant stars. In fact, very few iron species like FeCN, FeO, and FeH have been reported astronomically so far [35–40], although spectroscopic data from laboratory investigations exist for FeCN [41], FeNC [41], FeO [23], FeS [42], FeH [43], FeC [44], FeN [45], FeCl [46], and FeF [47], [48].

For the nucleosynthesis of iron isotopes in astrophysical objects, several different processes are involved [49, 50]. Measurements of the local isotopic ratio of iron isotopes in astronomical sources can be used to get more information about processes that take place in the inner part of the star and that may help to better determine the intrinsic physical properties which may be characteristic for different types of stars. The mass independent approach also allows to give accurate data of short lived Fe isotopologues, that are very difficult to measure in the laboratory. In particular, the radioactive ^{60}Fe isotope is of astrophysical relevance. Recently, Koll *et al.* [51] reported the detection of ^{60}Fe in the snow of Antarctica on earth. The authors concluded extraterrestrial dust from our solar neighbourhood as influx of this nucleus. ^{60}Fe is observed astrophysically in space via characteristic γ -ray emission lines at 1173 keV and 1333 keV, that are produced by radioactive β -decay from ^{60}Fe into ^{60}Co . [52]. The half-life of ^{60}Fe is $\tau_{1/2} = 2.62(4) \cdot 10^6 \text{ yr}$ ~~$\tau_{1/2} = 2.62(4) \cdot 10^6 \text{ a}$~~ [53]. The production of this nucleus is discussed for giant stars [54] and supernova explosions [55, 56].

However, the abundance is still not fully understood [57]. Recently Wang *et al.* [58] reported that the characteristic γ -ray emission of ^{60}Fe is too weak to spatially resolve its distribution in our galaxy. If radioactive isotopes have a sufficient long lifetime they can expand into cooler regions around their mother star where temperatures are low enough to form molecules. An example of this process is the recently detected radioactive ^{26}AlF in the shell of the merger CK Vulpeculae [59].

The observation of radioactive elements by γ -photons yields the absolute numbers of these elements. This is not possible, by means of rotational spectroscopy. Nevertheless, molecules continuously emit photons in the mm-wave region. Thus, the detection of rare isotopes may also be done by incorporating these elements as atomic component in molecules as complementary tool to observe γ -photons. FeO has already been reported astronomically [36, 37] and might be a good candidate for astronomical searches of radioactive ^{60}Fe .

2. Experimental Details

In our experiment, rotational transitions of iron monoxide were recorded using the Supersonic Jet Spectrometer for Terahertz Applications (SuJeSTA). The experiment has been described in detail elsewhere [29, 30]. In brief, the spectrometer consists of a synthesizer and multiplier chains (Virginia Diodes) to generate radiation in the millimetre/submillimetre region (250 GHz to 375 GHz). The radiation is guided through a multi-reflection cell, perpendicular to the supersonic jet and is then focused on a hot electron bolometer (QMC Instruments Ltd). Recorded signals are amplified and passed through a band-pass filter. The filtered signal is recorded with an USB-oscilloscope (Picoscope) connected to a personal computer.

Iron monoxide was produced in a laser ablation source, that is placed inside a vacuum chamber. The source consists of a pulsed gas valve (Parker series 9), a solid stainless steel source block, a target rod (solid iron with natural abundance of isotopes), electric motors for rotating and translating the target rod, and a 1064 nm Nd:YAG ablation laser operating at 30 Hz repetition rate. A gas mixture of 10 % oxygen in helium, at a stagnation pressure of 4 bar is used to generate a gas pulse of 2 ms duration. The 7 ns pulse of the Nd:YAG ablation laser is timed to coincide with the maximum gas flow at the target rod. Ablated iron interacts in a 6.2 mm long slit reaction channel (slit height of 1.0 mm and slit width of 12.0 mm) with the gas mixture. After passing the reaction channel, the gas forms a supersonic expansion into the vacuum chamber that is kept at a background pressure of typically 0.1 Pa. We also tested different designs of the reaction channel with lengths of 2.7 mm and 4.4 mm, but found that the 6.2 mm long channel yields highest amounts of iron monoxide. For comparison, Barnes *et al.* [13] used the same mixture, i.e. 90 % He and 10 % O_2 , in a laser ablation source with a 15 mm condensation tube for the production of iron monoxide. In our setup, before the gas mixture interacts with the laser ablation plasma, it is adiabatically cooled in a pre-expansion from an orifice of 0.79 mm^2 to a slit with an area of 12 mm^2 . Collisions and chemical reactions take place in the 6.2 mm long channel downstream. For an efficient reaction of laser ablated iron and cold oxygen it seems to be crucial that the collisions between the reagents take place in a somehow extended volume which is due to a longer reaction channel.

When measuring the rare ^{57}FeO and ^{58}FeO isotopologues, we frequently used the signal of the main isotopologue ^{56}FeO to optimise the molecule production. For the $^{56}\text{Fe}^{18}\text{O}$ isotopologue an enriched $^{18}\text{O}_2$ sample (Campro Scientific GmbH, 97 atom %)

Dataset	# transitions	isotopologues	method
This Work	16 [*]	⁵⁴ FeO, ⁵⁶ FeO, ⁵⁷ FeO, ⁵⁸ FeO, ⁵⁶ Fe ¹⁸ O	mm-wave
Allen ^a	79	⁵⁴ FeO, ⁵⁶ FeO	mm-wave
Endo ^b	6	⁵⁶ FeO	mm-wave
Kröckertskothén ^c	25	⁵⁶ FeO	mm-wave/ optical double resonance
Cheung ^d	1708 ^{**}	⁵⁶ FeO, ⁵⁴ FeO ^{***}	visible spectral region

^a Data taken from Allen *et al.* [25].

^b Data taken from Endo *et al.* [23].

^c Data taken from Kröckertskothén *et al.* [24].

^d Data taken from Cheung *et al.* [9, 10], see also [8].

^{*} For ⁵⁶Fe¹⁸O only transitions with J''=11 and J''=12 are used in the global analysis.

^{**} Energy levels from combination differences.

^{***} Not used in the global analysis.

Table 1. Datasets used in the Dunham-like analysis.

was used.

3. Results and Analysis

We measured 15 new transitions of the iron monoxide isotopologues ⁵⁷FeO (eight transitions), ⁵⁸FeO (two transitions), and ⁵⁶Fe¹⁸O (five transitions) and re-measured three transitions of ⁵⁶FeO and one transition of ⁵⁴FeO to compare absolute line positions and their accuracies with literature values, as shown in Table 2 and 3. As examples, two rotational transitions of the lowest $\Omega = 4$ state are displayed in Figure 1 and detailed views of the nuclear hyperfine splitting due to the nuclear spin of iron $I(^{57}\text{Fe}) = 1/2$ are given. To obtain centre line positions, we fitted Gaussian profiles to the measured lines. In addition we included data of ⁵⁶FeO and ⁵⁴FeO from the literature for the global analysis. The used datasets can be seen in Table 1. In total 126 pure rotational transitions and 1708 energy levels from combination differences are used in the fit. Our fit files and the complete list of lines included into the fit are available upon request. A calculated line list of the radioactive ⁶⁰FeO isotopologue can be found in Table 12.

Isotopically invariant fitting procedure

Before introducing the mass-independent procedure of FeO in its $X^5\Delta_i$ electronic ground state, a brief introduction of the used molecular parameters will be given.

The description of iron monoxide in a $^5\Delta$ electronic state by effective molecular parameters encompasses the rotational parameters (B_ν , D_ν), the spin-orbital parameters (A_ν , A_{D_ν} , η_ν), the spin-spin parameters (λ_ν , λ_{D_ν} , θ_ν , θ_{D_ν}), and the spin-rotational parameters (γ_ν , γ_{S_ν}). The parameters η_ν , θ_ν , θ_{D_ν} , γ_{S_ν} (see Brown and Carrington [60]) handle the higher order interactions caused by the high spin multiplicity of the state. In addition, Λ -splitting for a $^5\Delta$ electronic state is described by the parameters \tilde{m}_{Δ_ν} , \tilde{n}_{Δ_ν} , \tilde{o}_{Δ_ν} , and \tilde{p}_{Δ_ν} [61].

These fifteen effective molecular parameters are needed to describe iron monox-

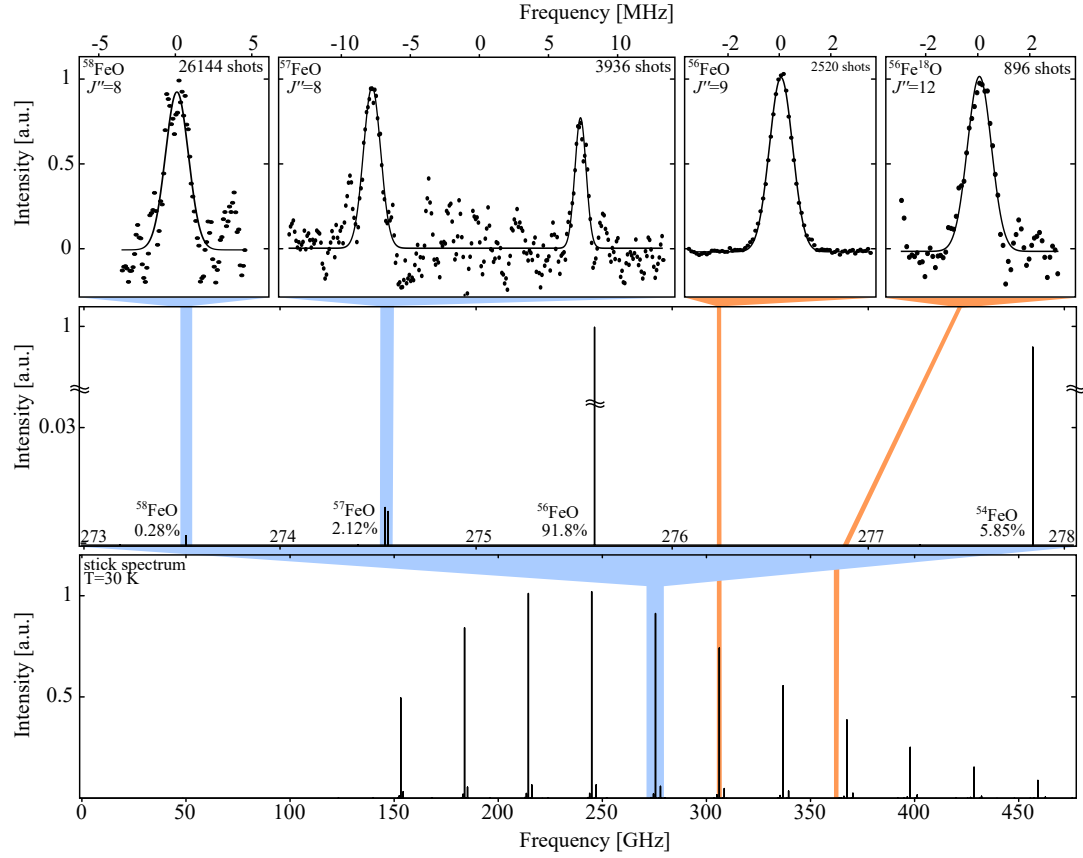


Figure 1. Simulated stick spectrum (lower panel), detail of the lower panel showing the different FeO isotopologues (middle panel), and typical measured lines for different isotopologues (upper panel). The $^{56}\text{Fe}^{18}\text{O}$ transition was measured using an $^{18}\text{O}_2$ enriched sample. For the measured lines, the laser shots per frequency point are depicted in the upper right corner.

J''	Ω''	ν_{obs} [MHz]	Allen <i>et al.</i> [25]
^{54}FeO			
8	4	277 839.933(16)	277 839.965(50)
^{56}FeO			
8	4	275 604.522(15)	275 604.520(50)
8	3	277 266.034(64)	277 266.040(50)
9	4	306 212.516(4)	306 212.518(50)
$^{56}\text{Fe}^{18}\text{O}$			
8	4	252 042.872(91)	
9	4	280 037.984(58)	
10	4	308 024.386(125)	
11	4	336 009.117(109)	
12	4	363 988.393(42)	
^{58}FeO			
8	4	273 519.545(100)	
9	4	303 896.497(87)	

Table 2. Observed rotational transitions of $^{54}\text{Fe}^{16}\text{O}$, $^{56}\text{Fe}^{16}\text{O}$, $^{58}\text{Fe}^{16}\text{O}$, and $^{56}\text{Fe}^{18}\text{O}$ with $\Delta J = 1$, $\Delta\Omega = 0$, and $\Delta F = 1$ transitions. 1σ uncertainties are given in parentheses.

J''	Ω''	F''	ν_{obs} [MHz]
8	4	8.5	274 536.010(82)
8	4	7.5	274 551.091(72)
9	4	9.5	305 027.426(64)
9	4	8.5	305 039.508(94)
10	4	10.5	335 513.504(45)
10	4	9.5	335 523.369(57)
11	4	11.5	365 995.004(52)
11	4	10.5	366 003.042(45)

Table 3. Observed rotational transitions of ^{57}FeO with $\Delta J = 1$, $\Delta\Omega = 0$, and $\Delta F = 1$ transitions. 1σ uncertainties are given in parentheses.

ide based on the used datasets. To evolve the mass-independent fit, correlated mass-independent parameters $\hat{O}_{k,l}$ need to be defined. In addition, the parameter $T_{\nu,\alpha}$ correlated to $U_{k,0}$ is introduced to account for the origin of the potential for isotopologues α , see Table 4.

In case of ^{57}FeO , where the hyperfine splitting is resolved, only the total diagonal hyperfine constant, h_4 , could be determined as only transitions with $\Omega = 4$ were observed.

In the present global analysis we included the microwave data of Endo *et al.* [23], Kröckertskothén *et al.* [24], and Allen *et al.* [25]. In addition vibrational data from the measurements of the 'orange band' system performed by Cheung *et al.* [10] have been used, which were assigned using combination differences [9, 10]. The ground state energy levels with respect to the vibrational excitation based on the LIF experiment [9] are determined and are included in the fitting procedure.

For the global fit of data the generalized equation for the Dunham-type multi-isotopologue analysis is used that has been previously described in Breier *et al.* [29, 30] and which was included into the software PGOPHER [62]

$$X_{\nu,\alpha} = \sum_k \left\{ \eta \cdot \mu_\alpha^{-\frac{2l+k}{2}} \cdot \hat{O}_{k,l} \cdot \left(1 + \sum_{i=A,B} \frac{m_e}{M_\alpha^i} \Delta_{\hat{O}_{k,l}}^i \right)_{\text{BO}} \cdot \left(\nu + \frac{1}{2} \right)^k \right\}. \quad (1)$$

Here in brief, the molecular parameter $X_{\nu,\alpha}$ of the isotopologue α in its vibrational state ν is represented by a sum over Dunham expansion terms (see Table 4). The index k denotes the ro-vibrational coupling order and l stands for the molecular parameter expansion order. Each term consists of five factors, the first one is the effective proportional factor η , which is necessary for the mass-independent description of hyperfine parameters. For FeO, this parameter is set to unity since only the ^{57}FeO rotational levels split into hyperfine patterns.

The second term of Eq. 1 represents the scaling factor of the reduced mass μ_α of the isotopologue α , i.e., $\mu = \frac{M^A M^B}{M^A + M^B}$ for the here investigated diatomic molecules AB. The next factor is the isotopic invariant fitting parameter $\hat{O}_{k,l}$ (see Tab. 4). The term in brackets is the Born-Oppenheimer correction (BO) factor of each isotopic invariant parameter. Here, m_e is the electron mass, M_α^i is either the mass of atom A or B with the corresponding $\Delta_{\hat{O}_{k,l}}^A$ or $\Delta_{\hat{O}_{k,l}}^B$ BO atomic scaling parameters. These parameters are determined from the first-order rotational expansion term U_{01} based on the available data. The last factor in Eq.1 describes the ro-vibrational coupling of the expansion terms. In our calculations we use the isotope masses of iron and oxygen as given by AME2016 [63].

The datasets of Table 1 are initially weighted by their experimental uncertainties. In addition, the dataset based on the 'orange band' [9, 10] is weighted by the factor $\sqrt{2}$ because of the combination differences. The 'orange band' is perturbed, which causes numerous outliers. The significance of these outliers for the fit is reduced by iterative weight adjustment of the datasets in each fitting attempt, known as the robust weighting method [64]. A similar iterative re-weighting procedure is included in PGOPHER. In this work the parameter ROBUST is chosen with a value of 8 so that the final weighted standard deviation value is almost unity. This treatment leads to the final fit weighted standard deviation value of 0.96. The averaged uncertainty of the rotational transitions is 59 kHz, matching the typical experimental uncertainties given

in the literature.

The mass-independent Dunham-like molecular parameters are shown in Table 5. In total 24 individual mass-independent parameters are used to describe all experimental datasets included into the fit.

4. Discussion and Conclusions

For comparison², the measured lines are listed in Table 2 together with those of Allen *et al.* [25]. The ro-vibrational resolved LIF data of $\nu = 0, 1, 2, 3$ measured by Cheung *et al.* [9] allows a mass-independent parametrisation and a direct comparison to our results, see Table 5. For the adaptation of parameters we used the equations given in Appendix A and the reduced mass of the ⁵⁶FeO isotopologue. We found the transformed parameters of Cheung *et al.* [9] in good agreement with our results.

The quality of the present dataset allows for the first time to determine Born-Oppenheimer breakdown (BOB) correction values of FeO. Compared to well behaved molecules which possess correction values in the order of unity, we found rather large $\Delta_{01}^{\text{Fe}} = -9.886(24)$ and $\Delta_{01}^{\text{O}} = -10.761(67)$ values for FeO. Similar values were found for other oxides, like TiO, but also for methylidyne, CH⁺ [66] (see Tab. 6). In the latter case a large rotational g_J factor increases the BOB correction terms [67], a mechanism that may also be relevant in the case of FeO which can not be proven since no experimental value for the g_J factor is available.

Furthermore, we calculated the equilibrium Born-Oppenheimer corrected bond length r_e^{BO} , the equilibrium bond length r_e , and the vibrational ground state bond length r_0 of the main isotopologue using the equations given in Appendix B. As can be seen from Table 7, the bond lengths r_e^{BO} and r_e agree to the third significant digit with the value of r_0 , indicating a rather harmonic vibrational potential. On the other hand, the BOB correction to the r_e bond length is rather large and of the order of 10^{-4} . For comparison, experimental values of Cheung *et al.* [9] and DFT calculations of Gutsev *et al.* [69] are also included in Table 7.

To compare the new molecular parameters to the literature but also to give user

²Allen *et al.* [25] measured absorption signals using a double pass optics through a Broida-type oven at static conditions. In this configuration only symmetric Doppler components are expected as have been seen. In contrast, our absorption signals were measured in perpendicular orientation to the supersonic jet expansion. Deviation from perpendicular configuration may result in a shift of the center frequency due to asymmetric Doppler components. However, a comparison of both datasets shows, that our lines match within a 1σ standard deviation and we concluded that the supersonic jet was perfectly aligned.

Table 4. Correlation of the commonly used molecular parameters $X_{\nu,\alpha}$ to mass-independent expanded Dunham parameters $\hat{O}_{k,l}$ and the effective proportional factor η as given in Eq. 1.

$X_{\nu,\alpha}$	$\hat{O}_{k,l}$	η	$X_{\nu,\alpha}$	$\hat{O}_{k,l}$	η	$X_{\nu,\alpha}$	$\hat{O}_{k,l}$	η
$T_{\nu,\alpha}$	$U_{k,0}$	1	A_D	$A_{k,1}$	1	λ	$\lambda_{k,0}$	1
$B_{\nu,\alpha}$	$U_{k,1}$	1	η	$\eta_{k,0}$	1	λ_D	$\lambda_{k,1}$	1
$D_{\nu,\alpha}$	$U_{k,2}$	1	$\tilde{m}_{\Delta,\nu,\alpha}$	$m_{\Delta,k,0}$	1	θ	$\theta_{k,0}$	1
$\gamma_{\nu,\alpha}$	$\gamma_{k,1}$	1	$\tilde{n}_{\Delta,\nu,\alpha}$	$n_{\Delta,k,1}$	1	θ_D	$\theta_{k,1}$	1
$\gamma_{S\nu,\alpha}$	$\gamma_{S_{k,1}}$	1	$\tilde{o}_{\Delta,\nu,\alpha}$	$o_{\Delta,k,2}$	1	$\tilde{p}_{\Delta,\nu,\alpha}$	$p_{\Delta,k,3}$	1
A	$A_{k,0}$	1						

Parameter	This Work	adapted from Cheung <i>et al.</i> [9]	Unit
$U_{00} \cdot 10^{-2}$	-4.391 705 9(56)		cm^{-1}
$U_{10} \cdot 10^{-3}$	3.105 007 06(85)	3.105 015 42(56)	$\text{cm}^{-1} \text{u}^{1/2}$
$U_{20} \cdot 10^{-1}$	-5.758 143(69)	-5.758 492(54)	$\text{cm}^{-1} \text{u}$
U_{01}	6.455 019(16)	6.451 974 63(82)	$\text{cm}^{-1} \text{u}$
$\Delta_{U_{01}}^{\text{Fe}}$	-9.886(24)		
$\Delta_{U_{01}}^{\text{O}}$	-10.761(67)		
$U_{11} \cdot 10^1$	-1.680 358(18)	-1.678 274(13)	$\text{cm}^{-1} \text{u}^{3/2}$
$U_{02} \cdot 10^4$	1.117 683(18)	1.120 80(32)	$\text{cm}^{-1} \text{u}^2$
$\gamma_{01} \cdot 10^1$	-3.868(17)		$\text{cm}^{-1} \text{u}$
$\gamma_{11} \cdot 10^2$	-2.445(23)		$\text{cm}^{-1} \text{u}^{3/2}$
$A_{00} \cdot 10^{-1}$	-9.492 425(14)	-9.490 930(22)	cm^{-1}
$A_{10} \cdot 10^2$	4.4454(88)	3.414(84)	$\text{cm}^{-1} \text{u}^{1/2}$
$A_{01} \cdot 10^5$	6.83(34)		$\text{cm}^{-1} \text{u}$
$\lambda_{00} \cdot 10^1$	9.480 10(76)		cm^{-1}
$\lambda_{10} \cdot 10^3$	-1.15(61)		$\text{cm}^{-1} \text{u}^{1/2}$
$\lambda_{01} \cdot 10^5$	-4.152(14)		$\text{cm}^{-1} \text{u}$
$\eta_{00} \cdot 10^2$	3.0224(15)	3.740(13)	cm^{-1}
$\theta_{00} \cdot 10^4$	-1.65(14)		cm^{-1}
$\theta_{01} \cdot 10^6$	6.403(37)		$\text{cm}^{-1} \text{u}$
$m_{00} \cdot 10^2$	-1.4697(11)		cm^{-1}
$n_{01} \cdot 10^4$	8.5241(15)		$\text{cm}^{-1} \text{u}$
$o_{02} \cdot 10^5$	-9.455(38)		$\text{cm}^{-1} \text{u}^2$
$p_{03} \cdot 10^5$	-3.559(50)		$\text{cm}^{-1} \text{u}^3$
$\gamma_{S,01} \cdot 10^4$	-1.1772(80)		$\text{cm}^{-1} \text{u}$

Table 5. Mass-independent Dunham-like molecular parameters of iron monoxide and adapted data from Cheung *et al.* [9] (see Appendix A). 1σ uncertainties are given in parentheses. The used datasets of this work are listed in Table 1.

Molecule (AB)	$\mu[\text{D}]$	Δ_{U01}^A	Δ_{U01}^B
$\text{FeO}(\text{X}^5\Delta)^a$	4.50(3)	−9.886(24)	−10.761(67)
$\text{TiO}(\text{X}^3\Delta)^b$	3.34(1)	−8.253(24)	−6.112(8)
$\text{CH}^+(\text{X}^1\Sigma^+)^c$	1.683	−7.975(11)	−9.226(8)

^a This work, but μ value taken from Steimle *et al.* [26].

^b Values taken from Steimle *et al.* [65] and Breier *et al.* [30].

^c Values taken from Cheng *et al.* [68] and Müller [66].

Table 6. Comparison of dipole moment and mass independent Born-Oppenheimer correction terms for $^{56}\text{Fe}^{16}\text{O}$, $^{48}\text{Ti}^{16}\text{O}$, and $^{12}\text{C}^1\text{H}^+$.

Parameter	This Work	Cheung <i>et al.</i> [9]	Gutsev <i>et al.</i> [69]
r_e^{BO}	1.616 030 2(20)		
r_e	1.616 406 882(17)	1.6164 ^a	1.613 ^b
r_0	1.619 399 315(15)	1.6194 ^a	

^a Exp.

^b B3LYP/ 6-311+G*.

Table 7. Molecular bond length of $^{56}\text{Fe}^{16}\text{O}$ in $\text{\AA} = 10^{-10} \text{ m}$. 1σ uncertainties are given in parentheses.

friendly values for further laboratory and possible astrophysical observations we present mass-dependent parameters of ^{56}FeO (Tab. 8), ^{54}FeO (Tab. 9), and ^{57}FeO (Tab. 10). Opposed to the results of Allen and co-workers [25], our global fit does not need any fixed parameters. For the rare isotopologues ^{58}FeO , ^{60}FeO , and $^{56}\text{Fe}^{18}\text{O}$ given in Table 11 there are no literature data to compare with. We used the results of Table 11 to calculate accurate transition frequencies of the astrophysical relevant ^{60}FeO , see Table 12. The presented result may also be useful to improve and test theoretical methods on iron bearing molecules.

Acknowledgement

TFG and co-workers would like to express their gratitude for 30 years of collaboration with Jürgen Gauss in the analysis of new molecules.

Funding

DFG priority program 1573 (Physics of the Interstellar Medium) under grants GI 319/3-1, GI 319/3-2, the University of Kassel through P/1052 'Programmlinie Zukunft', and CRC 1319 'ELCH'

Parameter	This Work	Allen <i>et al.</i> [25]
^{56}FeO		
$T \cdot 10^1$	-1.2328(53)	
$B \cdot 10^1$	5.168 121 097(23)	5.168 119 52(11)
$D \cdot 10^7$	7.224 49(12)	7.214 46(44)
$A \cdot 10^{-1}$	-9.491 795(14)	-9.494 635 ^a
$A_D \cdot 10^6$	5.49(37)	-80.1690(27)
$\eta \cdot 10^2$	3.0224(16)	3.5994(26)
$\gamma \cdot 10^2$	-3.137(14)	
$\gamma_S \cdot 10^6$	-9.465(64)	
$\lambda \cdot 10^1$	9.479 95(73)	9.3158 ^a
$\lambda_D \cdot 10^6$	-3.338(12)	-5.8839(20)
$\theta \cdot 10^4$	-1.65(14)	0.0 ^a
$\theta_D \cdot 10^7$	5.147(30)	3.886(16)
$\tilde{m} \cdot 10^2$	-1.4697(11)	-1.3261 ^a
$\tilde{n} \cdot 10^5$	6.853(12)	8.026(37)
$\tilde{o} \cdot 10^7$	-6.112(25)	-7.12(12)
$\tilde{p} \cdot 10^8$	-1.849(26)	

^a Fixed parameter.

Table 8. Molecular parameters of the main isotopologue ^{56}FeO in cm^{-1} . 1σ uncertainties are given in parentheses.

Parameter	This Work	Allen <i>et al.</i> [25]
^{54}FeO		
$T \cdot 10^1$	16.7402(54)	
$B \cdot 10^1$	5.210 535 097(50)	5.210 531 51(94)
$D \cdot 10^7$	7.343 83(12)	7.3283(25)
$A \cdot 10^{-1}$	-9.491 792(14)	-9.494 618 ^a
$A_D \cdot 10^6$	5.53(37)	-81.513(32)
$\eta \cdot 10^2$	3.0224(15)	3.598 66 ^a
$\gamma \cdot 10^2$	-3.163(14)	
$\gamma_S \cdot 10^6$	-9.542(65)	
$\lambda \cdot 10^1$	9.479 93(72)	9.319 21 ^a
$\lambda_D \cdot 10^6$	-3.365(12)	-5.925(16)
$\theta \cdot 10^4$	-1.65(14)	0.0 ^a
$\theta_D \cdot 10^7$	5.190(30)	3.9501 ^a
$\tilde{m} \cdot 10^2$	-1.4697(11)	-1.3261 ^a
$\tilde{n} \cdot 10^5$	6.910(12)	8.092 ^a
$\tilde{o} \cdot 10^7$	-6.212(25)	-7.238 ^a
$\tilde{p} \cdot 10^8$	-1.896(27)	

^a Fixed parameter.

Table 9. Molecular parameters of ^{54}FeO in cm^{-1} . 1σ uncertainties are given in parentheses.

Parameter	This Work	Barnes <i>et al.</i> [13]
^{57}FeO		
$T \cdot 10^1$	-9.7962(54)	
$B \cdot 10^1$	5.147 973 261(32)	5.088(3)
$D \cdot 10^7$	7.168 14(12)	
$A \cdot 10^{-1}$	-9.491 796(14)	
$A_D \cdot 10^6$	5.47(37)	
$\eta \cdot 10^2$	3.0223(15)	
$\gamma \cdot 10^2$	-3.125(32)	
$\gamma_S \cdot 10^6$	-9.428(95)	
$\lambda \cdot 10^1$	9.479 93(74)	
$\lambda_D \cdot 10^6$	-3.325(12)	
$\theta \cdot 10^4$	-1.65(14)	
$\theta_D \cdot 10^7$	5.127(30)	
$\tilde{m} \cdot 10^2$	-1.4697(12)	
$\tilde{n} \cdot 10^5$	6.826(12)	
$\tilde{o} \cdot 10^7$	-6.064(25)	
$\tilde{p} \cdot 10^8$	-1.828(26)	
$h_4 \cdot 10^3$	4.832(24)	$\leq 10.5^b$
$h^5_{\Delta_i} \cdot 10^3$		5.8(9) ^c

^a $h = a\Lambda + (b + c)\Sigma$.

^b Parameter in $^5\Delta_4$ component scaled from CoO and MnO, see Barnes *et al.* [13].

^c Parameter in the ground state $X^5\Delta_i$.

Table 10. Molecular parameters of ^{57}FeO in cm^{-1} . 1σ uncertainties are given in parentheses (This Work) and 3σ uncertainties (Barnes *et al.* [13]).

Parameter	^{58}FeO	^{60}FeO	$^{56}\text{Fe}^{18}\text{O}$
$T \cdot 10^1$	-18.0589(54)	-33.8412(54)	-195.1342(54)
$B \cdot 10^1$	5.128 570 194(48)	5.091 611 930(83)	4.721 577 9(13)
$D \cdot 10^7$	7.114 09(12)	7.011 69(12)	6.027 506(97)
$A \cdot 10^{-1}$	-9.491 797(14)	-9.491 799(14)	-9.491 822(14)
$A_D \cdot 10^6$	5.44(36)	5.41(36)	5.02(33)
$\eta \cdot 10^2$	3.0224(15)	3.0224(15)	3.0224(15)
$\gamma \cdot 10^2$	-3.113(13)	-3.091(13)	-2.865(12)
$\gamma_S \cdot 10^6$	-9.393(64)	-9.324(63)	-8.644(59)
$\lambda \cdot 10^1$	9.479 93(73)	9.479 94(74)	9.479 94(73)
$\lambda_D \cdot 10^6$	-3.312(11)	-3.288(11)	-3.049(11)
$\theta \cdot 10^4$	-1.65(14)	-1.65(14)	-1.65(14)
$\theta_D \cdot 10^7$	5.109(30)	5.071(30)	4.702(28)
$\tilde{m} \cdot 10^2$	-1.4697(11)	-1.4698(11)	-1.4697(11)
$\tilde{n} \cdot 10^5$	6.801(12)	6.751(12)	6.260(11)
$\tilde{o} \cdot 10^7$	-6.018(25)	-5.932(24)	-5.099(21)
$\tilde{p} \cdot 10^8$	-1.807(26)	-1.769(25)	-1.410(20)

Table 11. Molecular parameters of ^{58}FeO , ^{60}FeO , and $^{56}\text{Fe}^{18}\text{O}$ in cm^{-1} (this work). 1σ uncertainties are given in parentheses.

J'	J''	E' [K]	E'' [K]	ν [MHz]	$A_{ij} \cdot 10^3$ [s ⁻¹]
5	4	7.2418(6)	0.0000(6)	150 893.758(5)	0.13
6	5	15.9316(6)	7.2418(6)	181 067.562(6)	0.36
7	6	26.0695(6)	15.9316(6)	211 238.668(7)	0.70
8	7	37.6552(6)	26.0695(6)	241 406.625(9)	1.17
9	8	50.6885(6)	37.6552(6)	271 570.983(10)	1.79
10	9	65.1693(6)	50.6885(6)	301 731.290(11)	2.59
11	10	81.0974(6)	65.1693(6)	331 887.097(12)	3.58
12	11	98.4725(6)	81.0974(6)	362 037.952(13)	4.77
13	12	117.2943(6)	98.4725(6)	392 183.403(14)	6.20
14	13	137.5626(6)	117.2943(6)	422 322.999(15)	7.87
15	14	159.2771(6)	137.5626(6)	452 456.289(17)	9.81
16	15	182.4374(6)	159.2771(6)	482 582.819(18)	12.04
17	16	207.0433(6)	182.4374(6)	512 702.137(19)	14.58
18	17	233.0942(6)	207.0433(6)	542 813.789(21)	17.44
19	18	260.5899(6)	233.0942(6)	572 917.323(22)	20.64
20	19	289.5299(6)	260.5899(6)	603 012.283(24)	24.21

Table 12. Calculated rotational transitions of ⁶⁰FeO based on molecular parameters and calculated Einstein A_{ij} coefficients. Values and a model for the partition function Q can be found in the Appendix C. 1σ uncertainties are given in parentheses.

References

- [1] B. Rosen, *Nature* **156** (3967), 570–570 (1945).
- [2] R.K. Dhumwad and N.A. Narasimham, *Proceedings of the Indian Academy of Sciences - Section A* **64** (5), 283–290 (1966).
- [3] R.F. Barrow and M. Senior, *Nature* **223** (5213), 1359–1359 (1969).
- [4] P.S. Bagus and H.J.T. Preston, *The Journal of Chemical Physics* **59** (6), 2986–3002 (1973).
- [5] J.B. West and H.P. Broida, *The Journal of Chemical Physics* **62** (7), 2566–2574 (1975).
- [6] P.C. Engelking and W.C. Lineberger, *The Journal of Chemical Physics* **66** (11), 5054–5058 (1977).
- [7] D.W. Green, G.T. Reedy and J.G. Kay, *Journal of Molecular Spectroscopy* **78** (2), 257–266 (1979).
- [8] A.S.C. Cheung, R.M. Gordon and A.J. Merer, *Journal of Molecular Spectroscopy* **87** (1), 289 – 296 (1981).
- [9] A.C. Cheung, N. Lee, A. Lyyra, A. Merer and A. Taylor, *Journal of Molecular Spectroscopy* **95** (1), 213 – 225 (1982).
- [10] A.C. Cheung, A. Lyyra, A. Merer and A. Taylor, *Journal of Molecular Spectroscopy* **102** (1), 224–257 (1983).
- [11] T. Kröckertskothén, H. Knöckel and E. Tiemann, *Chemical Physics* **103** (2-3), 335–343 (1986).
- [12] Y. Azuma and A. Merer, *Journal of Molecular Spectroscopy* **135** (1), 194–196 (1989).
- [13] M. Barnes, M. Fraser, P. Hajigeorgiou and A. Merer, *Journal of Molecular Spectroscopy* **170** (2), 449–465 (1995).
- [14] J. Lei and P.J. Dagdigian, *Journal of Molecular Spectroscopy* **203** (2), 345–348 (2000).
- [15] I. Rahinov, A. Fomin, M. Poliak and S. Cheskis, *Applied Physics B* **117** (1), 317–323 (2014).
- [16] J.B. Kim, M.L. Weichman and D.M. Neumark, *Molecular Physics* **113** (15-16), 2105–2114 (2015).
- [17] A. Taylor, A.C. Cheung and A. Merer, *Journal of Molecular Spectroscopy* **113** (2), 487 – 494 (1985).
- [18] M. Krauss and W.J. Stevens, *The Journal of Chemical Physics* **82** (12), 5584–5596 (1985).
- [19] M. Dolg, U. Wedig, H. Stoll and H. Preuss, *The Journal of Chemical Physics* **86** (4), 2123–2131 (1987).
- [20] C.W. Bauschlicher and P. Maitre, *Theoretica Chimica Acta* **90** (2-3), 189–203 (1995).
- [21] O.V. Gornostaeva, V.M. Shatalov and Y.G. Pashkevich, *JETP Letters* **89** (4), 167–169 (2009).
- [22] C.N. Sakellaris, E. Miliordos and A. Mavridis, *The Journal of Chemical Physics* **134** (23), 234308 (2011).
- [23] Y. Endo, S. Saito and E. Hirota, *The Astrophysical Journal* **278**, L131 (1984).
- [24] T. Kröckertskothén, H. Knöckel and E. Tiemann, *Molecular Physics* **62** (4), 1031–1040 (1987).
- [25] M. Allen, L. Ziurys and J. Brown, *Chemical Physics Letters* **257** (1), 130 – 136 (1996).
- [26] T.C. Steimle, J. Gengler and P.J. Hodges, *The Journal of Chemical Physics* **121** (24), 12303 (2004).
- [27] S. Unterguggenberger, S. Noll, W. Feng, J.M.C. Plane, W. Kausch, S. Kimeswenger, A. Jones and S. Moehler, *Atmospheric Chemistry and Physics* **17** (6), 4177–4187 (2017).
- [28] J.R. de Laeter, J.K. Böhlke, P.D. Bièvre, H. Hidaka, H.S. Peiser, K.J.R. Rosman and P.D.P. Taylor, *Pure and Applied Chemistry* **75** (6), 683–800 (2003).
- [29] A.A. Breier, B. Waßmuth, T. Büchling, G.W. Fuchs, J. Gauss and T.F. Giesen, *Journal of Molecular Spectroscopy* **350**, 43–50 (2018).
- [30] A.A. Breier, B. Waßmuth, G.W. Fuchs, J. Gauss and T.F. Giesen, *Journal of Molecular Spectroscopy* **355**, 46–58 (2019).
- [31] M. Melosso, L. Bizzocchi, F. Tamassia, C. Degli Esposti, E. Canè and L. Dore, *Physical*

- Chemistry Chemical Physics **21** (7), 3564–3573 (2019).
- [32] E. Anders and N. Grevesse, *Geochimica et Cosmochimica Acta* **53** (1), 197–214 (1989).
 - [33] U.J. Sofia, J.A. Cardelli and B.D. Savage, *The Astrophysical Journal* **430**, 650 (1994).
 - [34] M. Asplund, N. Grevesse, A.J. Sauval and P. Scott, *Annual Review of Astronomy and Astrophysics* **47** (1), 481–522 (2009).
 - [35] L.N. Zack, D.T. Halfen and L.M. Ziurys, *The Astrophysical Journal* **733** (2), L36 (2011).
 - [36] C.M. Walmsley, R. Bachiller, G.P. des Forêts and P. Schilke, *The Astrophysical Journal* **566** (2), L109–L112 (2002).
 - [37] L. Decin, T. Danilovich, D. Gobrecht, J.M.C. Plane, A.M.S. Richards, C.A. Gottlieb and K.L.K. Lee, *The Astrophysical Journal* **855** (2), 113 (2018).
 - [38] H. Nordh, B. Lindgren and R.F. Wing, *Astronomy & Astrophysics* **56**, 1–6 (1977).
 - [39] R.E.S. Clegg and D.L. Lambert, *The Astrophysical Journal* **226**, 931 (1978).
 - [40] R.J. Hargreaves, K.H. Hinkle, C.W. Bauschlicher, S. Wende, A. Seifahrt and P.F. Bernath, *The Astronomical Journal* **140** (4), 919–924 (2010).
 - [41] M.A. Flory and L.M. Ziurys, *The Journal of Chemical Physics* **135** (18), 184303 (2011).
 - [42] S. Takano, S. Yamamoto and S. Saito, *Journal of Molecular Spectroscopy* **224** (2), 137–144 (2004).
 - [43] J.G. Phillips, S.P. Davis, B. Lindgren and W.J. Balfour, *The Astrophysical Journal Supplement Series* **65**, 721 (1987).
 - [44] M. Allen, T. Pesch and L.M. Ziurys, *The Astrophysical Journal Letters* **472** (1), L57 (1996).
 - [45] P.M. Sheridan, L.M. Ziurys and T. Hirano, *The Astrophysical Journal* **593** (2), L141–L144 (2003).
 - [46] M. Allen, B. Li and L. Ziurys, *Chemical Physics Letters* **270** (5), 517–526 (1997).
 - [47] M. Tanimoto, S. Saito and T. Okabayashi, *Chemical Physics Letters* **242** (1), 153 – 156 (1995).
 - [48] M.D. Allen and L.M. Ziurys, *The Journal of Chemical Physics* **106** (9), 3494–3503 (1997).
 - [49] S.E. Woosley and T.A. Weaver, *The Astrophysical Journal Supplement Series* **101**, 181 (1995).
 - [50] C. Iliadis, *Nuclear Physics of Stars*, 2nd ed. (Wiley-VCH, Weinheim, Germany, 2015).
 - [51] D. Koll, G. Korschinek, T. Faestermann, J. Gómez-Guzmán, S. Kipfstuhl, S. Merchel and J.M. Welch, *Physical Review Letters* **123** (7) (2019).
 - [52] W. Wang, M.J. Harris, R. Diehl, H. Hallouin, B. Cordier, A.W. Strong, K. Kretschmer, J. Knödlseider, P. Jean, G.G. Lichti, J.P. Roques, S. Schanne, A. von Kienlin, G. Weidenspointner and C. Wunderer, *Astronomy & Astrophysics* **469** (3), 1005–1012 (2007).
 - [53] G. Rugel, T. Faestermann, K. Knie, G. Korschinek, M. Poutivtsev, D. Schumann, N. Kivel, I. Günther-Leopold, R. Weinreich and M. Wohlmuther, *Physical Review Letters* **103** (7) (2009).
 - [54] M. Limongi and A. Chieffi, *Nuclear Physics A* **758**, 11–14 (2005).
 - [55] F.X. Timmes, S.E. Woosley, D.H. Hartmann, R.D. Hoffman, T.A. Weaver and F. Matteucci, *The Astrophysical Journal* **449**, 204 (1995).
 - [56] S. Wanajo, H.T. Janka and B. Müller, *The Astrophysical Journal* **774** (1), L6 (2013).
 - [57] A. Vasileiadis, Å. Nordlund and M. Bizzarro, *The Astrophysical Journal* **769** (1), L8 (2013).
 - [58] W. Wang, T. Siegert, Z.G. Dai, R. Diehl, J. Greiner, A. Heger, M. Krause, M. Lang, M.M.M. Pleintinger and X.L. Zhang, *The Astrophysical Journal* **889** (2), 169 (2020).
 - [59] T. Kamiński, R. Tylenda, K.M. Menten, A. Karakas, J.M. Winters, A.A. Breier, K.T. Wong, T.F. Giesen and N.A. Patel, *Nature Astronomy* **2** (10), 778–783 (2018).
 - [60] J.M. Brown and A. Carrington, *Rotational Spectroscopy of Diatomic Molecules* (Cambridge University Press, Cambridge, United Kingdom, 2003).
 - [61] J. Brown, A.C. Cheung and A. Merer, *Journal of Molecular Spectroscopy* **124** (2), 464 – 475 (1987).
 - [62] C.M. Western, *Journal of Quantitative Spectroscopy and Radiative Transfer* **186**, 221–242 (2017).

- [63] M. Wang, G. Audi, F.G. Kondev, W. Huang, S. Naimi and X. Xu, Chinese Physics C **41** (3), 030003 (2017).
- [64] J.K. Watson, Journal of Molecular Spectroscopy **219** (2), 326–328 (2003).
- [65] T.C. Steimle and W. Virgo, Chemical Physics Letters **381** (1), 30 – 36 (2003).
- [66] H.S.P. Müller, Astronomy & Astrophysics **514**, L6 (2010).
- [67] T. Amano, The Astrophysical Journal **716** (1), L1–L3 (2010).
- [68] M. Cheng, J.M. Brown, P. Rosmus, R. Linguerri, N. Komha and E.G. Myers, Physical Review A **75** (1) (2007).
- [69] G.L. Gutsev, B.K. Rao, P. Jena, The Journal of Physical Chemistry A **104** (22), 5374–5379, (2000).
- [70] A.A. Breier, Ph. D. thesis, *High-Resolution Microwave Spectroscopy of Radioactive Molecules* (kassel university press, Kassel, Germany, 2019).

5. Appendices

Appendix A. Dunham Parameter Adaptation

To compare our Dunham-like parameters to the values of Cheung *et al.* [9], we used the equations:

$$B_\nu = B_e - \alpha_e \left(\nu + \frac{1}{2} \right) \quad (\text{A1})$$

$$U_{01} = B_e \cdot \mu \quad (\text{A2})$$

$$U_{11} = -\alpha_e \cdot \mu^{3/2} \quad (\text{A3})$$

$$U_{20} = -\alpha_e \cdot \mu^{3/2} \quad (\text{A4})$$

$$T_\nu = \omega_e \left(\nu + \frac{1}{2} \right) - \omega_e x_e \left(\nu + \frac{1}{2} \right)^2 - \frac{\omega_e}{2} + \frac{\omega_e x_e}{4} \quad (\text{A5})$$

$$U_{10} = \omega_e \cdot \mu^{1/2} \quad (\text{A6})$$

$$U_{20} = -\omega_e x_e \cdot \mu \quad (\text{A7})$$

$$U_{30} = -\omega_e x_e \cdot \mu \quad (\text{A8})$$

$$D_\nu = D_e + \beta_e \left(\nu + \frac{1}{2} \right) \quad (\text{A9})$$

$$U_{02} = D_e \cdot \mu^2 \quad (\text{A10})$$

$$U_{12} = \beta_e \cdot \mu^{5/2} \quad (\text{A11})$$

$$A_\nu = A_e + A' \left(\nu + \frac{1}{2} \right) + A'' \left(\nu + \frac{1}{2} \right)^2 \quad (\text{A12})$$

$$A_{00} = A_e \quad (\text{A13})$$

$$A_{10} = A' \cdot \mu^{1/2} \quad (\text{A14})$$

$$A_{20} = A'' \cdot \mu^{3/2} \quad (\text{A15})$$

$$A_{30} = A''' \cdot \mu^{5/2} \quad (\text{A16})$$

$$\eta_\nu = \eta_e + \eta' \left(\nu + \frac{1}{2} \right) \quad (\text{A17})$$

$$\eta_{00} = \eta_e \quad (\text{A18})$$

$$\eta_{10} = \eta' \cdot \mu^{1/2} \quad (\text{A19})$$

Table C1. Calculated partition function Q for different temperatures T of ^{60}FeO .

T [K]	Q	T [K]	Q	T [K]	Q
1.6	0.193	90	250.189	200	732.038
3.2	2.109	100	284.560	210	787.729
6.4	8.945	110	320.689	220	845.470
10	18.006	120	358.642	230	905.272
20	44.761	130	398.470	240	967.143
30	72.086	140	440.208	250	1031.091
40	99.668	150	483.885	260	1097.124
50	127.682	160	529.523	270	1165.248
60	156.451	170	577.141	280	1235.468
70	186.297	180	626.757	290	1307.786
80	217.480	190	678.384	300	1382.206

Appendix B. Bond length calculations

To calculate the bond lengths r_e^{BO} , r_e , and r_0 from our parameters, we use the following equations [70]:

$$r_e^{\text{BO}} = \sqrt{\frac{16.85762918(29)}{U_{01}}} [\text{\AA}] \quad (\text{B1})$$

$$r_e = \sqrt{\frac{16.85762918(29)}{Y_{01}\mu_{56}}} [\text{\AA}] \quad (\text{B2})$$

$$Y_{01} = \frac{U_{01}}{\mu} \left(1 + \frac{m_e}{M_{\text{O}}} \Delta_{U_{01}}^{\text{O}} + \frac{m_e}{M_{\text{Fe}}} \Delta_{U_{01}}^{\text{Fe}} \right) \quad (\text{B3})$$

$$r_0 = \sqrt{\frac{16.85762918(29)}{B_0^{56}\mu_{56}}} [\text{\AA}] \quad (\text{B4})$$

Appendix C. Partition function for ^{60}FeO

The calculated partition function Q in Table C1 has been modelled with the following equation by the least squares fitting procedure. 1σ uncertainties are given in parenthesis:

$$Q(T) = p_1 T^3 + p_2 T^2 + p_3 T + p_4 \quad (\text{C1})$$

$$p_1 = 8.27(57) \cdot 10^{-6} \text{ K}^{-3} \quad (\text{C2})$$

$$p_2 = 5.40(25) \cdot 10^{-3} \text{ K}^{-2} \quad (\text{C3})$$

$$p_3 = 2.264(31) \text{ K}^{-1} \quad (\text{C4})$$

$$p_4 = -3.24(94) \quad (\text{C5})$$